# 21.5 An LTE-Harvesting BLE-to-WiFi Backscattering Chip for Single-Device RFID-Like Interrogation

Shih-Kai Kuo*, Manideep Dunna*, Hongyu Lu, Akshit Agarwal, Dinesh Bharadia, Patrick P. Mercier

University of California, San Diego, CA
*Equally Credited Authors (ECAs)

2023 IEEE International Solid- State Circuits Conference (ISSCC) | 978-1-6654-9016-0/23/$31.00 ©2023 IEEE | DOI: 10.1109/ISSCC42615.2023.10067815

Recent work in backscatter modulation has enabled very low-power communication between an IoT tag and commodity hardware such as WiFi or BLE transceivers [1-4], enabling a new set of exciting IoT applications such as on-body sensors or asset trackers that demand low power and low deployment cost via compatibility with existing standards. However, such backscatter approaches tend to require two external devices: a transmitting tone generator [3,5] or access point (AP) [1,2,4] and a receiving AP [1-5] in order to perform tone-to-WiFi [3,5], WiFi-to-WiFi [1,2,4] or BLE-to-BLE [4] communication without requiring power-expensive RF signal generation on the backscattering IoT tag (Fig. 21.5.1, top). Unfortunately, not all applications natively have multiple available APs, and deployment of additional infrastructure can be expensive. Since there are few, if any, commodity devices that feature full-duplex communication or multiple radios operating concurrently with the same standard in the same band, a low-power backscatter IC that can be interrogated by a single device has not been demonstrated. In addition, most such backscattering IoT tags require either batteries or auxiliary energy harvesters, which can further increase deployment and/or maintenance costs.

This paper presents a backscattering IC that can enable wireless communication and battery-less operation with multi-standard inputs coming from only a single mobile device by: 1) harvesting power from LTE signals; 2) buffering this power onto a energy storage capacitor; 3) starting-up a duty-cycled WiFi wake-up receiver (WuRX) that is then re-purposed to detect the timing of incident BLE packets; and 4) transforming a tone-like bit-repetition BLE packet into a single-side-band (SSB) QPSK modulated 802.11b WiFi packet via a fully-reflective I/Q backscatter modulator, as illustrated in Fig. 21.5.1 (bottom). In this manner, the energy harvesting source is directly coupled to the intent to interrogate, unlike other sources of energy harvesting that may or may not be available at interrogation time (e.g., PV, TEG) and therefore require an energy buffering battery. As a result, this approach enables a robust, low-cost, and scalable way to provide power and enable communication in an RFID-like manner, but in this case when utilizing existing commodity mobile devices that feature separate LTE, WiFi, and BLE chips as a reader.

Inspired by [6], the incident tone for backscatter modulation can be generated by intentionally transmitting a BLE packet with either all 1s or all 0s. To avoid channel uncertainty due to frequency hopping, this work leverages only BLE advertisement packets on ch. 37, 38 and 39. The most basic way to perform DSSS backscattering for compatibility with 802.11b is to modulate the incident tone with baseband data that is multiplied with an 11MHz Barker code. However, doing so would cause the backscatter signal to land on the same frequency as the incident tone; since BLE and WiFi channels do not share the same center frequency, this is not possible within the confines of the two standards (never mind the self-interference problems that would also occur). Therefore, an intermediate frequency (IF) for channel shifting is required, which has to be carefully chosen to enable frequency translation between one of the three possible BLE advertisement channels and multiple different WiFi channels.

To generate the required 11MHz clock for the Barker code processor and the required IF frequency ($\Delta f$) for channel shifting simultaneously, a common multiple of these two frequencies is generated by an FLL-stabilized ring oscillator, whose output is then divided by M to generate 11MHz, and N to generate $\Delta f$ (Fig. 21.5.2, top), where M and N are integers. Because BLE utilizes FSK modulation with one of the tones set 0.25MHz away from its center frequency, the offset frequency, $\Delta f$, from the BLE tone to the WiFi center frequency must be $x$.25MHz or $x$.75MHz, where $x$ is an integer. Under these conditions, the minimum value of N must be 4, and the 8 possible values that M can take to enable BLE to WiFi channel translation are shown in Fig. 21.5.2 (middle right). For example, to translate from BLE ch. 38 to WiFi ch. 11, M=13, $\Delta f$=35.75MHz, and $f_{RO}$=143MHz. The FLL is only active for 0.915ms to save power.

Figure 21.5.2 (bottom) shows the timing of the tag operation. Its capacitively-buffered power supply is first charged by LTE signals transmitted by the interrogating mobile device. After charging, the tag has to wake up and synchronize with the mobile device. To accomplish this, the mobile device first transmits a WiFi CTS-to-self packet to temporarily clear up the WiFi channel that will be used to receive the backscattered packet, followed by transmission of two WiFi packets with pre-specified lengths and gaps that the on-chip WuRx energy detects. At this point, the FLL is activated for timing gap $t_1$, which is long enough to calibrate the ring oscillator. After this the FLL is shut down, and BLE tone-modified advertisement packets of length 2.12ms (the maximum programmable BLE5 packet length) are transmitted sequentially on ch. 37, 38, and 39. To generate the WiFi packet, which is shorter than the BLE packet, a timing gap $t_2$ has to be determined carefully. This is accomplished by reusing the WiFi WuRX's comparator to determine the rising edge of each BLE packet and selecting the appropriate one to begin the backscatter operation based on the desired channel translation parameters.

The block diagram of the backscatter chip is shown in Fig. 21.5.3. Here, a 5-stage Dickson rectifier is used to harvest incident LTE energy, and a voltage sensor detects when the output voltage of the rectifier reaches 1V. At this point, an LDO is turned on, which acts as the power supply for the remaining blocks. An envelope detector (ED) and a comparator are used to sense when the 32.768kHz crystal oscillator, which is powered by $VDD_{LDO}$, starts up. Once the 32.768kHz clock is established, an ED-first wake-up receiver with a counter-based correlator [2,4] wakes up the tag when it detects the incident WiFi signals with pre-defined lengths and gaps. When the wake-up signal is pulled high, the ring oscillator is turned on. To combat PVT variation, a successive approximation register (SAR) FLL, consisting of a time counter which calculates the divided ring oscillator frequency $f_{RO}$, and a SAR control block which generates the coarse and fine-tuning bits along with a fine-tuned voltage divider for the ring oscillator, is used to calibrate the output frequency to the desired value. Half the crystal oscillator frequency is used as the FLL reference to calculate the $f_{RO}$ error. The calibration process finishes in 15 cycles, which takes 0.915ms. The FLL is disabled afterward, and the calibrated digital control codes are fixed and stored in the control block when the tag is performing backscattering. Previous backscatter work has shown that an open-loop ring oscillator has sufficient short-term stability to enable successful 802.11b backscattering [3]. Finally, backscattering is achieved via a fully reflective transmission-line-less reflector [4] using the outputs of the baseband Barker code processor.

The proposed backscatter IC was fabricated in 65nm, occupying a core area of 0.43 mm$^2$. Figure 21.5.4 (top left) shows how the 100nW crystal oscillator starts up within 2.5s after incident power arrival. The chip consumes 4.5μW during wake-up mode, and 15μW during IF clock calibration. During active backscattering mode, the chip consumes an active power of 25μW. Since wake-up, frequency calibration, and then backscattering take 1-to-2ms, and considering the energy consumption of the crystal oscillator, a 1μF 0402 ceramic capacitor offers sufficient energy density when charged to 1V to enable a full backscattering routine, even if no additional LTE energy is harvested. The remaining plots in Fig. 21.5.4 demonstrate how the chip can take in BLE tone packets at all three advertisement channels, and generate frequency-translated packets to 8 different 802.11b WiFi channels using the integer-N arithmetic on-chip. Wireless experiments in Fig. 21.5.5 (top) demonstrate successful energy harvesting from an LTE transmitter, reception of WiFi wake-up packets from a WiFi transmitter, reception of BLE tone packets from a BLE transmitter, and reflected and modulated WiFi packets for reception by a WiFi receiver - all of which could easily be located on a single mobile device. The range of operation is limited by the LTE energy harvester, but as shown in Fig. 21.5.5 (bottom) can still operate over 50cm, which is adequate for many applications such as on-body sensors, smart robotics, asset management during deliveries, etc., where a single commodity mobile device is waved in the vicinity of the tag instead of a dedicated RFID reader and power transfer device. In all cases at 50cm and below, the charging time takes less than 1s before backscatter operation can begin.

Figure 21.5.6 compares results to prior-art tone- and BLE-to-WiFi backscatter systems. The proposed design is the first integrated, self-sustainable backscatter tag that can operate from a single mobile device that features LTE, BLE, and WiFi chips on it. A die micrograph is shown in Fig. 21.5.7.

*Acknowledgement:*
This work was supported in part by the National Science Foundation under Grant 1923902 and UC San Diego Center for Wearable Sensors.

*References:*
[1] P.-H. Wang et al., “A 28μW IoT Tag that can Communicate with Commodity WiFi Transceivers via a Single-Side-Band QPSK Backscatter Communication Technique,” *ISSCC*, pp. 312-313, Feb. 2020.
[2] M. Meng et al., “Improving the Range of WiFi Backscatter Via a Passive Retro-Reflective Single-Side-Band-Modulating MIMO Array and Non-Absorbing Termination,” *ISSCC*, pp. 202-203, Feb. 2021.
[3] L. Lin et al., “Battery-Less IoT Sensor Node with PLL-Less WiFi Backscattering Communications in a 2.5-μW Peak Power Envelope,” *VLSI Symp.,* 2021.
[4] S. -K. Kuo et al., “A WiFi and Bluetooth Backscattering Combo Chip Featuring Beam Steering via a Fully-Reflective Phased-Controlled Multi-Antenna Termination Technique Enabling Operation Over 56 Meters,” *ISSCC*, pp. 366-367, Feb. 2022
[5] B. Kellogg et al., “Passive Wi-Fi: Bringing Low Power to Wi-Fi Transmissions.” 13th USENIX Symposium on Networked Systems Design and Implementation (NSDI 16). 2016.
[6] V. Iyer et al., “Inter-technology backscatter: Towards internet connectivity for implanted devices.” *Proc. of the 2016 ACM SIGCOMM Conference*, 2016.

Authorized licensed use limited to: Univ of Calif San Diego. Downloaded on August 02,2023 at 16:49:41 UTC from IEEE Xplore. Restrictions apply.

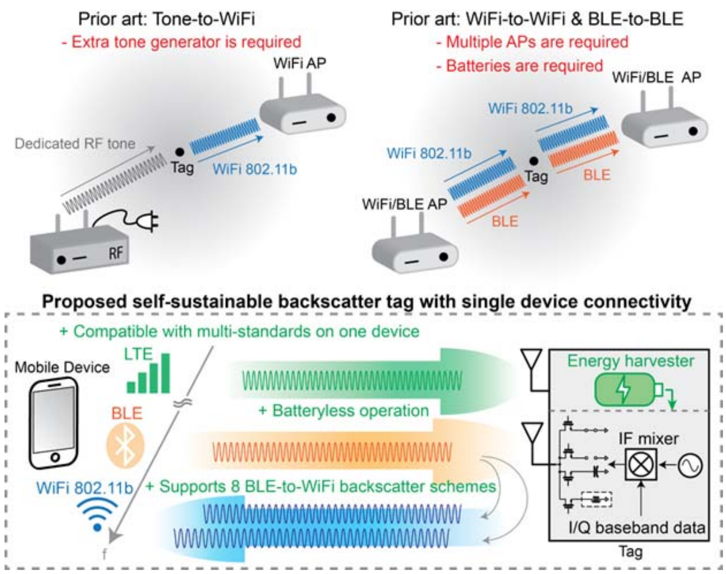


Figure 21.5.1: Prior-art WiFi and BLE-based backscatter approaches (top); proposed self-sustaining single-interrogation-device backscatter system (bottom).

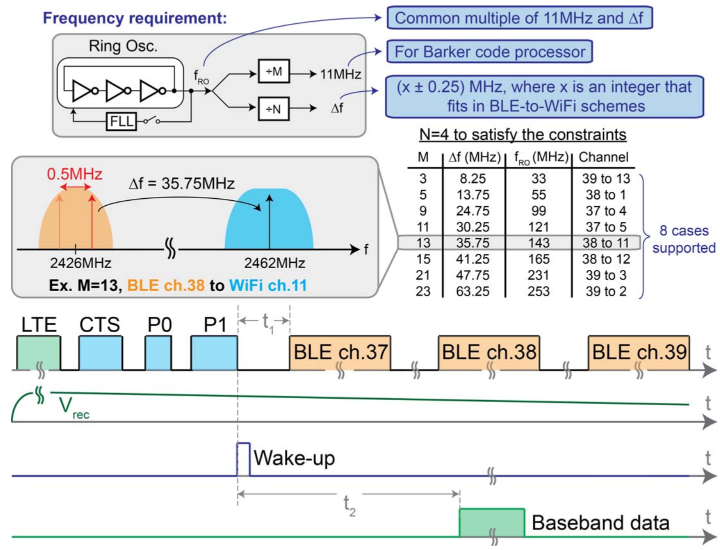


Figure 21.5.2: Frequency planning to enable translation from all possible BLE advertisement channels to up to 8 different WiFi channels (top); operation timing diagram (bottom).

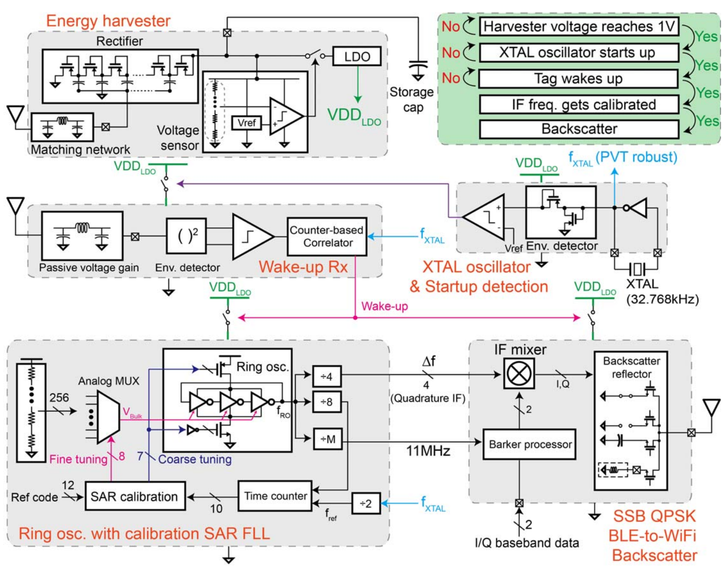


Figure 21.5.3: Block diagram of the tag, including LTE energy harvesting and power management, WiFi wake-up, crystal oscillator, ring oscillator, and reflector stages.

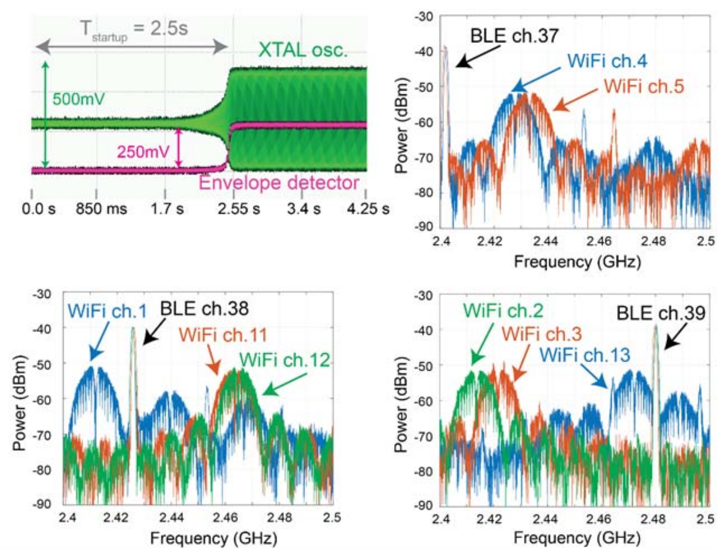


Figure 21.5.4: Measured crystal oscillator startup transients and measured spectra showing frequency translation from three BLE advertisement channels to fully modulated WiFi signals at 8 different WiFi channels.

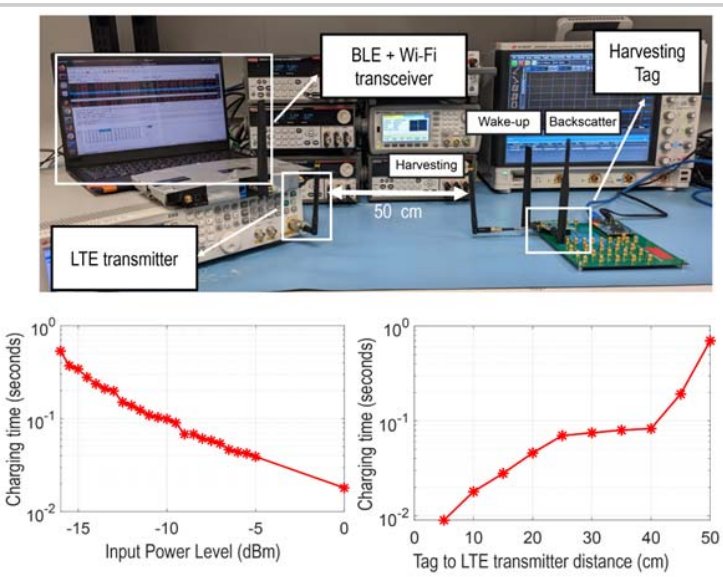


Figure 21.5.5: Photograph of the wireless testing setup (top); measured wireless charging time vs. input power level and distance (bottom).

| | [3] VLSI'21 | [6] SIGCOMM'16 | [5] NSDI'16 | [1] ISSCC'20 | [2] ISSCC'21 | [4] ISSCC'22 | This Work |
|---|---|---|---|---|---|---|---|
| Technology | 180 nm | No chip | No chip | 65 nm | 65 nm | 65 nm | 65 nm |
| Core Area ($mm^2$) | 1.62 | No chip | No chip | 0.34 | 0.41 | 0.42 | 0.43 |
| Backscatter Scheme | Tone to WiFi 802.11b | SSB BLE tone to WiFi 802.11b | Tone to WiFi 802.11b | WiFi 802.11b to WiFi 802.11b | WiFi 802.11b to WiFi 802.11b | WiFi 802.11b to WiFi 802.11b | **SSB BLE tone to WiFi 802.11b** |
| Single Side Band? | No | Yes | No | Yes | Yes | Yes | **Yes** |
| Max Data Rate | 1 Mbps | 11 Mbps | 11 Mbps | 2 Mbps | 2 Mbps | 2 Mbps | 2 Mbps |
| Incident Source | Tone Generator | BLE | Tone Generator | WiFi | WiFi | WiFi | **BLE** |
| Self-sustainability | No | No | No | No | No | No | **Yes** |
| On-chip backscatter frequency tunability | No* | - | - | No | No | No | **Yes**** |
| Wake-up Power (µW) | 0.15 | No | 18 (COTS devices) | 2.8 | 4.5 | 5.5 | 4.5 |
| Backscatter Communication Power (µW) | 2.5* | 28 (Simulated) | 59.2 (Simulated) | 28 | 32 | 39 | 25 |

* Only generates an 11MHz clock which requires a dedicated input tone that is not BLE-synthesizable.

** 8 BLE-to-WiFi cases are supported.

Figure 21.5.6: Table of comparisons to other tone/BLE-to-WiFi works.

Authorized licensed use limited to: Univ of Calif San Diego. Downloaded on August 02,2023 at 16:49:41 UTC from IEEE Xplore. Restrictions apply.

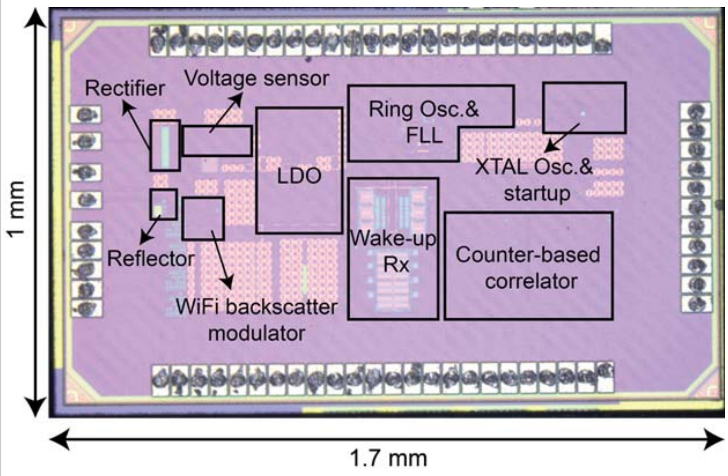


**Figure 21.5.7: Die micrograph of the proposed single-device-interrogated LTE-powered BLE-to-WiFi backscattering chip.**

Authorized licensed use limited to: Univ of Calif San Diego. Downloaded on August 02,2023 at 16:49:41 UTC from IEEE Xplore. Restrictions apply.



978-1-6654-9016-0/23/$31.00 ©2023 IEEE